Behavior of sodium atomic vapor in optical cavities below the threshold for bistability

W. E. Schulz,* W. R. MacGillivray, and M. C. Standage

School of Science, Griffith University, Nathan, 4111 Australia

(Received 28 January 1987)

A study is presented of the transmission characteristics of low-finesse ring and Fabry-Perot optical cavities containing sodium vapor and operated below the threshold for optical bistability. Novel features are observed in the transmission signals obtained as the laser light frequency is swept through resonance with a sodium D transition. The ring cavity transmission peaks display a broad absorption profile except for the peak which is tuned to the center of the profile which is almost completely transmitted. A similarly tuned cavity transmission peak in the Fabry-Perot étalon is split into three, with the central peak being very narrow. A theoretical description for each cavity is developed in terms of a Λ-type, three-state model for the atomic energy levels associated with the transition. Using parameter values based on the experimental conditions, theoretical transmission signals for the linear cavity are obtained which are in good detailed agreement with the experimental results. For the ring cavity, agreement is also good except for the degree of absorption of the central peak.

I. INTRODUCTION

Optical cavities with sodium atomic vapor as an intracavity medium have been the subject of a variety of experiments in the last ten years. First came the observation of optical bistability in a Fabry-Perot étalon filled with sodium vapor.[1] Other work investigating the behavior of similar systems has included the detection of bistability in a pseudo-two-level atomic medium created by power and collisional broadening,[2] the lowering of the threshold for low- to high-branch switching by optical pumping in the presence of magnetic fields,[3-5] the observation of bistability in a ring cavity,[6] and the recording of critical slowing down[7] when the system is subjected to a fast light pulse and the injected power approached the switching threshold. Tristability[8,9] and self-pulsing[10] have also been observed in linear cavities filled with sodium vapor and subjected to magnetic fields.

With the exception of the work of Ref. 2, these experiments have exploited the multistate nature of the energy levels associated with the sodium D lines. A manifestation of this multistate behavior was reported by us[6] in the preliminary results of experiments involving sodium vapor as the medium in both a linear and a ring cavity under conditions below the threshold for bistability. A major difference in the behavior of the two cavity systems was observed in their respective transmissions when the frequency of the injected radiation was swept through a D line. For the ring cavity, the transmission peaks displayed the absorption profile of the atomic transition, except for the peak which was tuned to the center of this profile. This central peak was almost completely transmitted. A similarly tuned transmission peak in the Fabry-Perot étalon did not have enhanced transmission but rather was split into three, with the central peak being very narrow. A tentative hypothesis based on a Λ-type, three-state model for the energy levels associated with the D transition was made. Subsequently, we discussed[11] an attempt to model the ring cavity transmission with a medium of

such atoms, including inhomogeneous broadening. However, due to an incorrect application of the mean-field approximation, the qualitative behavior of two-state and three-state atoms in the ring cavity was found to be similar. This similarity is removed with the correct use of the approximation which is detailed in Sec. III C 1.

Recently, a theory has been developed which describes the behavior of inhomogeneously broadened, Λ-type, three-state atoms with nondegenerate lower states interacting with single-mode, plane-wave light in a Fabry-Perot étalon.[12] Computer simulations of the transmission of the étalon including only the dispersive part of the refractive index as calculated by this theory have displayed the same general form as the reported experimental data.[6] In Sec. III C 2, this theory is extended to include absorption and coupling between the atomic ground states.

This paper, then, deals in some detail with the behavior of atomic sodium vapor in optical cavities below the threshold for optical bistability. In Sec. II the experiments are briefly described and the data are presented. Section III consists of the development of a theory to describe the behavior of both types of optical cavities in terms of a Λ-type, three-state atomic model. The simulated cavity transmissions and the experimental data are compared in Sec. IV.

II. EXPERIMENT

Details of the experiment setup have been given previously[6,11] and so only a brief resume is presented here. The optical cavity consisted of either a two-mirror Fabry-Perot étalon or a three-mirror ring cavity. All mirrors were flat and the input and output mirrors had reflectivities of 93%. For tuning and fine alignment of the cavities, one mirror was mounted on a piezoelectric translator. The free-spectral range of the linear cavity was approximately 980 MHz and that of the ring cavity 700 MHz. Their finesse, when the injected light was detuned from the atomic resonances, was between five and nine.

The sodium was contained in a Pyrex glass cell which was heated. Thermocouples were attached at various points to the outside surface of the cell and, while only allowing an approximate estimate of the absolute vapor temperature (to within about 20%), they were quite adequate for indicating more accurately the changes in vapor temperature. The light source was a Spectra Physics 380A ring dye laser pumped by a Spectra Physics 164 Ar^+ laser. Up to 200 mW was available at the input mirror of the optical cavity in a collimated beam with a $1/e$ diameter of 1 mm typically. In the case of the Fabry-Perot étalon, an optical isolator prevented retroreflections to the laser. The light path through the cell was 2.5 cm long. The central region of the transmitted light was detected by a photomultiplier tube and recorded on a storage oscilloscope. Synchronous ramping of the laser frequency and the oscilloscope x plates generated pictures of cavity transmission as a function of laser frequency.

Figures 1 and 2 are of transmission data collected from the systems for conditions below the threshold for bistability. In both cases, the temperature increases from the top to the bottom picture. The ring cavity data (Fig. 1) was recorded for the laser tuned to the D_2 transition and
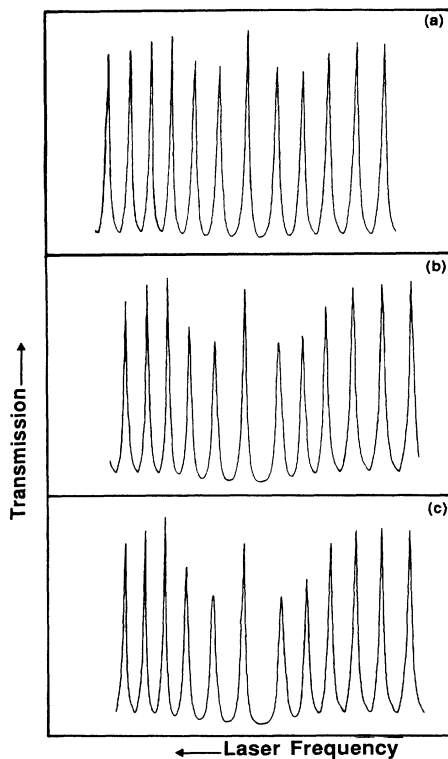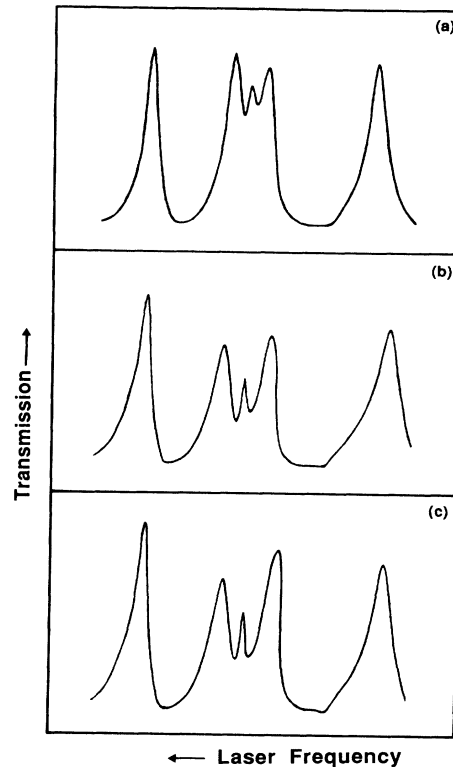

FIG. 2. The Fabry-Perot étalon transmission data under conditions similar to Fig. 1. The central feature of the triple peak is at the frequency midway between the ground-state transitions. The temperature of the vapor is slightly less than in Fig. 1 and the temperature range of the sequence is about 10 °C. Linearly polarized light of whole beam intensity of 130 mW was injected into the cavity, whose characteristics were a finesse of 5 and a free-spectral range of 980 MHz.

FIG. 1. Transmission of a low-finesse $(F = 6)$ ring optical cavity filled with sodium vapor vs laser-frequency tuning about the D_2 transition as a function of temperature. The temperature range was estimated as 140 to 155 °C to within 20%. The whole-beam-injected intensity was 95 mW. The cavity had a free-spectral range of about 700 MHz. The enhanced peak in the center of the absorption profile was tuned to the frequency midway between the two ground-state hyperfine transitions.

an injected intensity of 95 mW. The temperature range was estimated to be 140–155 °C. Except for the central peak, the cavity transmission peaks within the Doppler profile decrease with increasing atomic density. However, for these low atomic densities, the central peak, which is tuned to a frequency approximately halfway between the frequencies of the transitions from the two ground-state hyperfine levels, remains at nearly 100% transmission.

The transmission of the linear cavity displays markedly different behavior. Figure 2 is recorded data for scanning the frequency of the laser through three étalon peaks about the maximum of the D_2 line-absorption profile with 130 mW of injected light. The temperature of the vapor changed by 10 °C through the sequence with a mean-absolute temperature less than that measured for the ring cavity data. The center peak is split into three subpeaks, the outer two of which are pushed outwards as the atomic density increases. The inner subpeak has a width much narrow than the other profiles and is located at the absorption maximum. This central feature appeared for both the D_1 and D_2 transitions and was independent of the polarization of the incident light, indicating that this phenomenon appears to be independent of the hyperfine

structure of the upper level.

In the ring optical cavity, the transmitted light represents the sum of traveling waves that have propagated through the atomic medium and been filtered by the cavity. Thus, the relative peak heights in the transmission reflect the absorption profile of the intracavity medium. The inference drawn from the data of Fig. 1 is that the transition is not exhibiting behavior consistent with a two-level atomic system where the absorption would be a maximum at the center. As well, for atomic sodium vapor at these temperatures, the Doppler width of an absorption profile is about 1.5 GHz. The width of the total absorption profile of the ring cavity transmission (neglecting the presence of the central peak) is approximately 3.0 GHz. Together, these two observations suggest that the absorption profile is due to two, slightly overlapping, two-level systems. Several configurations of atomic energy levels could give rise to such an absorption profile including the so-called Λ system where two ground states of slightly differing energy are connected to the same excited state.

III. THEORY

A. Energy-level model

The structure of the lowest energy levels of ^{23}Na is depicted in Fig. 3.[13] Each hyperfine level is $2F + 1$ degenerate so that, for example, a detailed model for the D_2 transition would have to include 16 upper states and 8 lower states. This number of states makes calculations using this model unfeasible when the parameters have to be averaged over the velocity distribution and then used to calculate the field from Maxwell's equations with appropriate boundary conditions. A simple model is re-
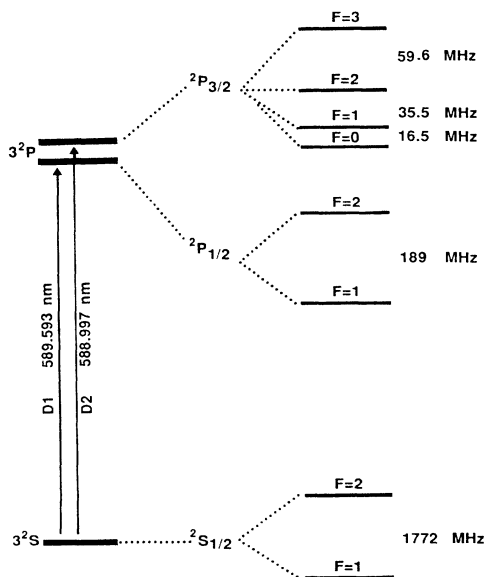
quired and, as implied in Sec. II, the one chosen is the three-state, Λ-type configuration with nondegenerate ground states as shown in Fig. 4.

The dipole moments of the optically allowed transitions $|1\rangle - |3\rangle$ and $|2\rangle - |3\rangle$ are taken as equal and it is assumed that there is equal probability of state $|3\rangle$ relaxing to state $|2\rangle$ or state $|1\rangle$. For sodium vapor at the temperatures used in the experiments of Sec. II, spontaneous emission dominates the relaxation process. Transitions between the two ground states are not optically allowed, but a redistribution between them can occur within the ensemble of atoms due to collisions and ground-state atoms entering the laser beam path. No relaxations out of the system are allowed, that is, the system is closed.

This model for these energy levels has been used previously,[14] however some justification for it under the experimental conditions of Sec. II follows. The essence of the argument is that there is significant mixing of the excited-state hyperfine levels due to power broadening and of the magnetic states within a level due to a residual magnetic field.

Power broadening δv_p is related to the transition Rabi frequency v_R by[15]

$$\delta v_p = \sqrt{2} v_R . \tag{1}$$

Using an estimate of the peak intracavity intensities of 100 mW/mm^2, the Rabi frequencies of transitions between magnetic hyperfine states associated with the D_1 line range from approximately 80 to 200 MHz while, for the D_2 line, the range is 40 MHz–280 MHz. Considering that the frequency splitting of the excited-state hyperfine levels is 189 MHz for the D_1 transition and that 60 MHz is the largest splitting in the D_2 excited-level manifold, significant overlapping of the transitions to these levels would be expected at these intensities. On the other hand, the transitions from the ground-state hyperfine levels are separated by 1772 MHz and so no overlapping would occur for a single atom, although, in the ensemble of atoms, both transitions lie within the overall Doppler profile.

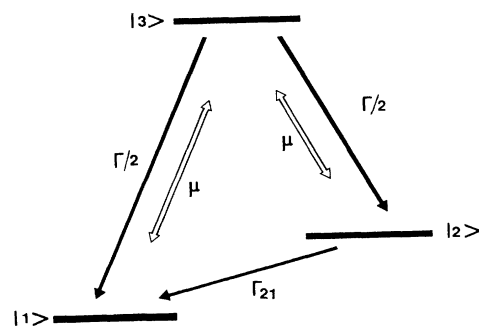Since low-finesse cavities were used in the experiments

FIG. 3. Fine and hyperfine structure of the lowest-energy levels of ^{23}Na showing the wavelengths of the D transitions and the hyperfine-levels separation frequency values (Ref. 13).

FIG. 4. The Λ-type, three-state model for the sodium D transitions with nondegenerate ground states ($|1\rangle$ and $|2\rangle$), equal dipole moments (μ) for transitions to the excited state ($|3\rangle$), and equal rates of excited-state relaxation ($\Gamma/2$). Coupling between the ground states is at a rate of Γ_{21}.

reported here, the power broadening at the lowest intra-cavity intensity is still significant. For a cavity with a finesse of 10, the power broadening at the lowest intensity is one-fifth of that at the peak intensity, while for the lowest finesse used (approximately 5) the broadening only decreases by one half. The implication of these estimates taken in combination with the data of Fig. 1 is that the simplest model appropriate for the sodium D transitions under the conditions of these experiments is a three-state, Λ-type energy-level configuration with nondegenerate ground states.

Further, the approximation of equal dipole moments for the two optically allowed transitions arises from the observation of optical nutations in an atomic beam apparatus.[16] It was found that for each D line, the Rabi frequencies associated with the two ground-state to excited-state transitions $(F=1\rightarrow F'$ and $F=2\rightarrow F')$ were equal to within 10% measuring error. Also from this data, the relaxation rates from the excited state to each ground state were estimated to be the same, but with less accuracy.

No attempt was made in the experiments to nullify the magnetic field of the earth which was approximately transverse to the direction of propagation of the light with magnitude of 0.6 G. Its presence will cause a mixing of the magnetic hyperfine substates. As was noted in Sec. II, there was no qualitative difference observed in the transmission data of the Fabry-Perot étalon system when injected with either circularly or linearly polarized light. This observation is interpreted as a direct result of the mixing of the magnetic hyperfine substates.

Thus, it would appear that the simple three-level model described above should be a reasonable approximation for the energy levels associated with the sodium D lines under the experimental conditions described in Sec. II and we now proceed to the development of an appropriate theoretical description.

B. The density matrix

We consider an ensemble of Λ-type, three-level atoms interacting with a classical, traveling plane wave propagating in the z direction whose form is written as

$$E=\tfrac{1}{2}E_0\exp[i(\omega_L t -kz)]+\text{c.c.} \ , \tag{2}$$

where

$$E_0=|E_0|\exp(i\phi) \ . \tag{3}$$

Since we neglect polarization effects in our model, the inclusion of the vectorial properties of parameters such as the radiation field and the atomic dipole moment are not necessary. The atomic response is described by the density matrix ρ_{ij} whose component equations, after the rotating-wave approximation has been made, are given by[14,17,18]

$$\dot{\rho}_{33}=-2\operatorname{Im}(\alpha\tilde{\rho}_{13})-2\operatorname{Im}(\alpha\tilde{\rho}_{23})-\rho_{33}/T_1 \ , \tag{4a}$$

$$\dot{\rho}_{22}=2\operatorname{Im}(\alpha\tilde{\rho}_{23})-(1/\tau)(\rho_{22}-\rho_{11})+\rho_{33}/2T_1 \ , \tag{4b}$$

$$\dot{\rho}_{11}=2\operatorname{Im}(\alpha\tilde{\rho}_{13})+(1/\tau)(\rho_{22}-\rho_{11})+\rho_{33}/2T_1 \ , \tag{4c}$$

$$\dot{\tilde{\rho}}_{13}=-(1/T_2+i\Delta)\tilde{\rho}_{13}-i\alpha^*(\rho_{11}-\rho_{33})-i\alpha^*\tilde{\rho}_{12} \ , \tag{4d}$$

$$\dot{\tilde{\rho}}_{23}=-(1/T_2+i\Delta')\tilde{\rho}_{23}-i\alpha^*(\rho_{22}-\rho_{33})-i\alpha^*\tilde{\rho}_{21} \ , \tag{4e}$$

$$\dot{\tilde{\rho}}_{12}=-(1/\tau-i\omega_{21})\tilde{\rho}_{12}+i\alpha^*\rho_{32}-i\alpha\tilde{\rho}_{13} \ , \tag{4f}$$

with, in addition, the relationship

$$\tilde{\rho}_{ij}^*=\tilde{\rho}_{ji} \ . \tag{4g}$$

The detuning terms are given by

$$\Delta=\omega_L-kv-\omega_{31} \ , \tag{5a}$$

$$\Delta'=\omega_L-kv-\omega_{32} \ , \tag{5b}$$

where v is the component of the atomic velocity in the z direction and k is the wave number. For spontaneous emission, the relaxation terms are related by

$$T_1=T_2/2=1/\Gamma \ , \tag{6}$$

while $1/\tau(\Gamma_{21})$ is the rate of redistribution between the ground states. The complex variable α is half the Rabi frequency expressed in radians per second

$$\alpha=\frac{\mu E_0}{2\hbar} \ . \tag{7}$$

Thus α can be written in the form

$$\alpha=\alpha_0\exp(i\phi) \ , \tag{8}$$

where

$$\alpha_0=\frac{\mu|E_0|}{2\hbar} \ . \tag{9}$$

The condition of closure for the system is expressed by the relation

$$\operatorname{tr}\rho=\rho_{11}+\rho_{22}+\rho_{33}=1 \ . \tag{10}$$

Finally, the usual transformation to the rotating frame for the off-diagonal elements ρ_{i3} has been made, viz.,

$$\rho_{i3}=\tilde{\rho}_{i3}\exp[i(\omega_L t -kz)] \ , \tag{11}$$

with

$$\rho_{12}=\tilde{\rho}_{12} \ . \tag{12}$$

For the purposes of this study, only the steady-state solutions are required. Gaussian elimination techniques can be used to solve Eqs. (4) coupled with Eq. (10). The solutions for the off-diagonal elements $\tilde{\rho}_{i3}$ have the functional form

$$\tilde{\rho}_{i3}=\alpha^*f_i(|\alpha|) \ , \tag{13}$$

whereas all other terms contain α in modulus form only. So all calculations were carried out for a real field $|E_0|$ and then multiplied by the appropriate phase factor. In practice, the analytic solutions are cumbersome and offer no significant advantage in computational speed over a numerical method of solution. A Gaussian elimination algorithm with backward substitution was used.

The role of the ground-state coupling in the model is illustrated in Fig. 5. Here the dispersion and absorption of the atomic medium, i.e., the real and imaginary parts of $\tilde{\rho}_{31}+\tilde{\rho}_{32}$ respectively, are plotted against the laser detuning for various values of τ. A field strength of $\alpha=10^7$
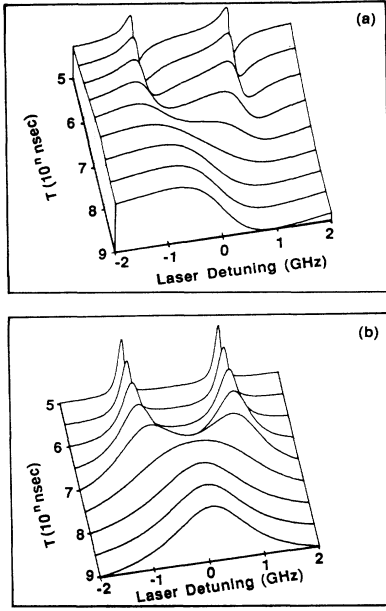
FIG. 5. (a) Dispersion and (b) absorption vs laser detuning for a Λ-type, three-state atomic model as a function of ground-states coupling time τ. A half Rabi frequency term of $\alpha = 10^7$ rad sec^{-1} was used in the calculation as well as the sodium relaxation times in the spontaneous emission limit of $T_1 = 16$ nsec and $T_2 = 32$ nsec. The vertical axis is normalized for each plot. The laser detuning is defined to be zero at the frequency midway between the two atomic transition frequencies.

rad/sec was used in the calculation to minimize power-broadening effects so as to highlight the three-state behavior. Parameter values relevant to the sodium D lines were substituted. For values of τ greater than 100 msec, the atoms exhibit the properties of a broad, two-state system but as τ decreases below 1 msec, the $|1\rangle$-$|3\rangle$ and $|2\rangle$-$|3\rangle$ transitions become clearly decoupled. In this latter case, the rate of optical pumping between the ground states is less than the rate of their population redistribution.

The macroscopic response of the medium at point z of the light path is found by averaging the component solutions over the ensemble-velocity distribution which is taken to be Maxwellian. Hence

$$\rho_{ij}(z) = \int_{-\infty}^{\infty} \rho_{ij}(v,z) g(v) dv , \tag{14}$$

where the weighting function is given by

$$g(v) = \exp(-v^2/v_0^2)/(v_0\sqrt{\pi}) , \tag{15}$$

where v_0 is the most probable velocity.

The polarization induced in the medium by the field is

$$P = N \mathrm{tr}(\hat{\rho}\hat{\mu}) , \tag{16}$$

where N is the atomic number density, $\hat{\rho}$ is the density operator, and $\hat{\mu}$ is the dipole-moment operator. Evaluation of the trace yields P of the form

$$P = \tfrac{1}{2}P_0 \exp[i(\omega_L t - kz)] + \mathrm{c.c.} , \tag{17}$$

where

$$P_0 = 2N\mu[\tilde{\rho}_{31}(z) + \tilde{\rho}_{32}(z)] . \tag{18}$$

Thus from Eq. (13), P_0 has the form

$$P_0 = P(|E_0|) \exp(i\phi) . \tag{19}$$

The polarization acts as the source term for the field in Maxwell's wave equation, which, in the slowly varying amplitude approximation[19] can be written as

$$\frac{dE_0}{dz} = \frac{i\omega_L}{2\epsilon_0 c} P_0 . \tag{20}$$

C. The optical cavities

1. Ring cavity

To model the steady-state response of a ring cavity with a medium consisting of an ensemble of three-state atoms, Eq. (20) must be solved for the field following substitution for the polarization P_0 from Eq. (18) and then invoking the boundary conditions at the input ($z = 0$) and output ($z = L$) mirrors given by,[20] respectively,

$$E_0(z = 0) = \sqrt{T}E_I + R \exp(i\Delta_c t_c)E_0(z = L) , \tag{21a}$$

$$E_T = \sqrt{T}E_0(z = L) , \tag{21b}$$

where $E_0(z)$ is the field amplitude inside the cavity and E_I and E_T are the incident and transmitted field amplitudes. The input and output mirrors are assumed to have the same reflectivity R and transmittivity T, while the other mirrors which constitute the ring have reflectivities of 100%. t_c is the round-trip time and Δ_c is the cavity detuning from the incident light,

$$\Delta_c = \omega_L - \omega_c , \tag{22}$$

so that $\Delta_c t_c$ is the phase mismatch for one round trip in an empty cavity. The medium occupies the space between the input and output mirrors. Substituting Eqs. (3) and (19) into Eq. (20) yields

$$\frac{d}{dz}|E_0| + i|E_0|\frac{d\phi}{dz} = \frac{i\omega_L}{2\epsilon_0 c}[P(|E_0|)] , \tag{23}$$

which is equivalently written

$$\frac{d}{dz}|E_0| = -\frac{\omega_L}{2\epsilon_0 c}\mathrm{Im}[P(|E_0|)] , \tag{24a}$$

$$\frac{d\phi}{dz} = \frac{\omega_L}{2\epsilon_0 c}\mathrm{Re}[P(|E_0|)]/|E_0| . \tag{24b}$$

This system is formally integrated from $z = 0$ to $z = L$ giving

$$|E_0(z)| \big|_0^L = -\frac{\omega_L}{2\epsilon_0 c}\int_0^L \mathrm{Im}[P(|E_0|)]dz , \tag{25a}$$

$$\phi(z) \big|_0^L = \frac{\omega_L}{2\epsilon_0 c}\int_0^L \{\mathrm{Re}[P(|E_0|)]/|E_0(z)|\}dz . \tag{25b}$$

The mean-field approximation[21] is made by assuming that the polarization is constant for the field strengths involved. The expressions then become

$$|E_0(L)| - |E_0(0)| = -\frac{\omega_L L}{2\epsilon_0 c} \text{Im}[P(|E_0|)] \, , \qquad (26a)$$

$$\phi(L) - \phi(0) = \frac{\omega_L L}{2\epsilon_0 c} \text{Re}[P(|E_0|)]/|E_0| \, . \qquad (26b)$$

For computational convenience, $|E_0(L)|$ is chosen to calculate the polarization. Thus, given an output field E_T, $E_0(0)$ is calculated and hence the incident field E_I is found from Eq. (21a). If the external parameters such as laser frequency, atomic density, etc., are appropriately chosen, a plot of $|E_T|$ versus $|E_I|$ will take the form of the "S-curve" signature of bistability. However, for the purpose of this work, the parameter values are deliberately chosen to keep the system below the threshold for bistability.

In practice, most calculations are performed in terms of the Rabi frequency rather than the field amplitude. Substituting Eq. (18) for P_0 into Eq. (20) and multiplying by $\mu/2\hbar$ gives

$$\frac{d}{dz}\alpha(z) = \frac{i\omega_L \mu^2 N}{2\epsilon_0 c\hbar}(\tilde{\rho}_{31} + \tilde{\rho}_{32}) \, . \qquad (27)$$

In state equations of this type, it has been traditional to express the density parameter in terms of the cooperativity parameter C.[22] For a two-state system

$$C = \alpha_{\text{abs}} L/2T \, , \qquad (28)$$

where the two-state absorption coefficient is given by

$$\alpha_{\text{abs}} = \frac{\omega_L \mu^2 T_2 N}{2\hbar\epsilon_0 c} \, . \qquad (29)$$

Substitution of Eqs. (29) and (28) into Eq. (27) yields

$$\frac{d}{dz}\alpha(z) = i\frac{2CT}{LT_2}(\tilde{\rho}_{31} + \tilde{\rho}_{32}) \, . \qquad (30)$$

This is merely a formal substitution of two-state system parameters and they have no direct physical interpretation in the three-state system. Rather, it is a convenient form of Eq. (20) in which C remains as a free parameter in the calculations. In particular, C is used merely as a measure of the atomic density. No attempt has been made to calculate an effective $C^{2,23}$ in the presence of inhomogeneous broadening. Therefore the threshold for bistability does not correspond to $C = 4$ in our three-state calculations.

2. The Fabry-Perot étalon

The theory for an ensemble of two-state atoms in a Fabry-Perot étalon using explicit Maxwell-Bloch equations and field boundary conditions has received considerable attention.[24] However, attempts to utilize these approaches for three-state systems proved to be not possible either from a physical or from a numerical point of view.[25] In the model developed in this section, we consider the boundary conditions implicitly by calculating the response of the three-state atoms to a standing-wave field

$$E = \tfrac{1}{2}E_0[\cos(\omega_L t - kz) + \cos(\omega_L t + kz)] \, . \qquad (31)$$

The field E can be written in the form

$$E = \tfrac{1}{2}E_1 \exp(i\omega_L t) + \text{c.c.} \, , \qquad (32)$$

where the field amplitude E_1 is expressed as

$$E_1 = E_0 \cos(kz) \, . \qquad (33)$$

By writing the z coordinate as an explicit function of time,

$$z = vt + z_0 \, , \qquad (34)$$

where v is the z component of the atomic velocity, and defining terms ω and ψ such that

$$\omega = \omega_L v/c \qquad (35)$$

and

$$\psi = \omega_L z_0/c \, , \qquad (36)$$

Eq. (33) becomes

$$E_1 = E_0 \cos(\omega t + \psi) \, . \qquad (37)$$

The Rabi frequency term α is now time dependent and is given by

$$\alpha(t) = \alpha_0 \cos(\omega t + \psi) \, , \qquad (38)$$

where α_0 is half the steady Rabi frequency component and is given, in terms of E_0, by Eq. (9). The transmission I_r of the Fabry-Perot étalon, expressed as the ratio of transmitted intensity over incident intensity, is given by

$$I_r = \frac{A(1-R)^2}{(1-RA)^2 + 4RA\sin^2\theta} \, , \qquad (39)$$

where A is an attenuation coefficient. We consider only absorption-free mirrors and so the attenuation is determined by the atoms only. In the weak-absorption limit, A can be written as

$$A = \exp[-\omega_M \chi''/(2\Phi)] \qquad (40)$$

(where Φ is the free-spectral range) whereas the half-round-trip phase shift θ is expressed as

$$\theta = (\delta + \tfrac{1}{2}\omega_M \chi')/(2\Phi) \, . \qquad (41)$$

The complex susceptibility has been defined as

$$\chi = \chi' + i\chi'' \qquad (42)$$

and the detuning δ is

$$\delta = \omega_L - \omega_M \, , \qquad (43)$$

where ω_M is the frequency midway between the two atomic transition frequencies and is the frequency to which the cavity is tuned. Details of the derivation of Eqs. (39)–(41) are given in the Appendix.

Finally, R is the ratio of the reflected intensity to incident intensity at each mirror and is assumed to be the same for each mirror. It is related to the cavity finesse F by

$$F = \pi\sqrt{R}/(1-R) \, . \qquad (44)$$

The susceptibility is related to the positive-frequency amplitude of the macroscopic polarization P_1 by

$$\chi = P_1 / \epsilon_0 E_1 , \tag{45}$$

which, in turn, can be shown to be related to the now time-dependent off-diagonal density-matrix elements $\tilde{\rho}_{3i}(t)$ in the form of Eq. (18). Here the transformation for these off-diagonal elements is

$$\rho_{3i} = \tilde{\rho}_{3i}(t) \exp(-i\omega_L t) . \tag{46}$$

Writing the Doppler integration explicitly and substituting for E_1 in terms of the half Rabi frequency α, Eq. (45) becomes

$$\chi = \frac{N\mu^2}{\epsilon_0 \hbar v_0 \sqrt{\pi}} \int_{-\infty}^{\infty} \frac{\tilde{\rho}_{31}(v,t) + \tilde{\rho}_{32}(v,t)}{\alpha} \exp(-v^2/v_0^2) dv . \tag{47}$$

The density-matrix component equations can no longer be solved in the usual way by taking the rotating-wave approximation since the transformed Hamiltonian is still oscillating with frequency ω. However, component values can be found by solving Eqs. (4) in the steady state after making the case $2(b)$ substitutions of Ref. 12,

$$\alpha \rightarrow \alpha_I / 2 , \tag{48a}$$

$$\Delta \rightarrow \Delta_b = \Delta_{ND} + \omega + (\alpha_I/2)^2 \left[\frac{\omega + \Delta_{ND} + 2\Delta'_{ND}}{(\Delta_{ND} - \omega)(\Delta'_{ND} + \omega)} \right] , \tag{48b}$$

$$\Delta \rightarrow \Delta'_b = \Delta'_{ND} - \omega - (\alpha_I/2)^2 \left[\frac{\omega - 2\Delta_{ND} - \Delta'_{ND}}{(\Delta_{ND} - \omega)(\Delta'_{ND} + \omega)} \right] , \tag{48c}$$

where

$$\alpha_I = \sqrt{I_r} \alpha_0 \tag{49}$$

is the steady part of the half Rabi frequency weighted for the relative intensity inside the cavity and Δ_{ND} and Δ'_{ND} are the detunings given by Eqs. (5) but without the Doppler term kv. The density-matrix components $\tilde{\rho}^b_{3i}(\omega)$ are related to those in Eq. (47) by the transformations

$$\tilde{\rho}_{32} = \tilde{\rho}^b_{32} \exp[i(\omega t + \psi)] , \tag{50a}$$

$$\tilde{\rho}_{31} = \tilde{\rho}^b_{31} \exp[-i(\omega t + \psi)] . \tag{50b}$$

By neglecting the oscillating terms, the expression (47) for the susceptibility can be written as

$$\chi = \frac{2k}{\omega_M} \int_0^{\infty} \frac{\tilde{\rho}^b_{31}(\omega) + \tilde{\rho}^b_{32}(\omega)}{\alpha_I} \exp(-\omega^2/\omega_D^2) d\omega , \tag{51}$$

with

$$k = \frac{N\mu^2 \omega_M}{\epsilon_0 \hbar \omega_D \sqrt{\pi}} , \tag{52}$$

and ω_D is the $1/e$ width of the Doppler profile. Thus, by evaluating the relevant terms, the implicit equation for I_r, Eq. (39), can be solved numerically by an iterative

method.

IV. RESULTS OF CALCULATIONS AND DISCUSSION

Figure 6 shows simulated transmissions of the ring cavity as the frequency of the laser field is swept through the two transitions of the three-state atom ensemble. The parameter values are listed in the figure caption. The center cavity transmission peak is tuned to the frequency f_M midway between the two transitions and the laser frequency is expressed as a detuning from this value. The sequence is for increasing atomic density represented by the parameter C. The values of C were chosen to obtain approximate agreement between the computed and experimental data for the absorption of the cavity peaks adjacent to the center peak. By substituting appropriate
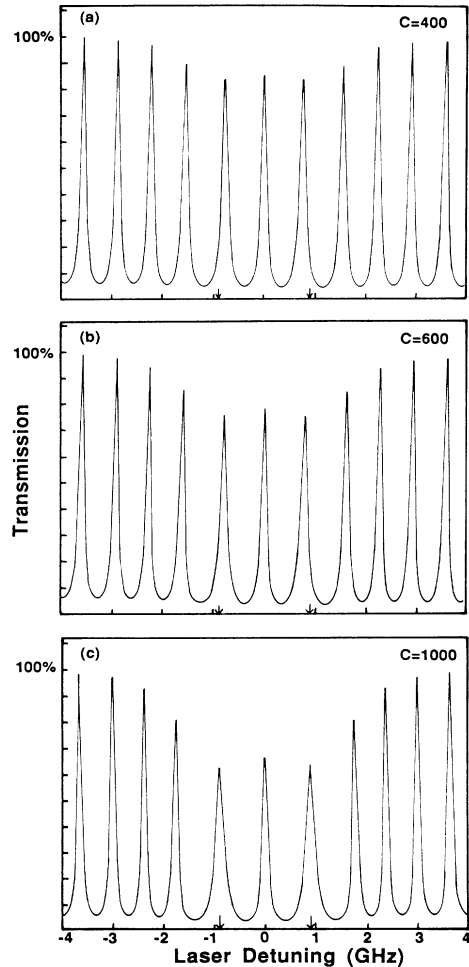
FIG. 6. Simulated transmission of a ring cavity vs laser detuning calculated in the mean-field limit for a peak intracavity Rabi frequency of 100 MHz. The zero-detuning point is the frequency midway between the two transitions which are 886 MHz to each side (arrows). Other parameters are $T_1 = 16$ nsec, $T_2 = 32$ nsec, $\tau = 1$ μsec, finesse $= 6$, $\Phi = 700$ MHz, and Doppler width $= 1.5$ GHz. (a) $C = 400$, (b) $C = 600$, and (c) $C = 1000$.

values into Eqs. (28) and (29), the atomic density range estimated for these plots is $3.5 \times 10^{11} - 8.8 \times 10^{11}$ cm^{-3}. This corresponds to a temperature range of 162–178 °C which agrees quite well with the experimentally estimated temperature range.

Comparison of Fig. 6 with Fig. 1 shows that, with the exception of the degree of transmission of the central peak, the three-state model reproduces the general behavioral trends of the experimental data. The reduced transmission of the ring cavity peaks within three free-spectral ranges of the center is seen in both the experimental and the simulated data. Also evident in both is the small-frequency shifting of the cavity peaks away from the center as the density is increased.

The transmission of the simulated center peak is enhanced when compared with those next to it, but to nowhere near the same extent as is evident in the experimental data. The values of the Doppler width, intracavity Rabi frequency, and ground-states coupling time were varied in an attempt to obtain from the calculations greater transmission of the center peak but only small changes were produced. The single-transition Doppler width of 1.5 GHz is appropriate for atomic sodium at the estimated vapor temperatures. Lower values of intracavity Rabi frequency did give a calculated central peak of slightly greater transmission but reduced the frequency shifting of the other peaks. On the other hand, intracavity Rabi frequencies of greater than 100 MHz for these cavity parameters reduced the transmission of the center peak to approximately that of the next peaks. A value of 100 MHz for the intracavity Rabi frequency is not an unreasonable estimate considering the experimentally deduced value of the intracavity intensity. The value of the ground-states coupling time τ of 1 μsec was chosen after consideration of the most probable atomic velocity at the vapor temperature ($\sim$500 m/sec) and the laser beam diameter ($\sim$0.5 mm).

The results of the calculations for the transmission of the Fabry-Perot étalon are shown in Fig. 7. Again, the central cavity profile is tuned to f_M and the laser-field frequency is swept through a little more than three free-spectral ranges about this profile. The parameter values are given in the figure caption.

Overall, the numerically simulated transmissions match the experimental transmissions of Fig. 2 quite accurately. The center profile is split to become triple peaked. As the density increases, the entire central profile becomes broader and its transmission decreases with the center one of its peaks more absorbed than the outer two. As well, the central feature narrows with increasing density.

The value of the peak intracavity Rabi frequency, 180 MHz, was chosen so that the ratio of the width of the entire central profile to the widths of the other cavity peaks in the simulation was approximately the same as that recorded by the experiment. This value falls within the range of the experimental estimates. The Fabry-Perot experiments were carried out using a higher-laser intensity than that used in the ring cavity (see Sec. II) although the difference was not as great as that used in the calculations.

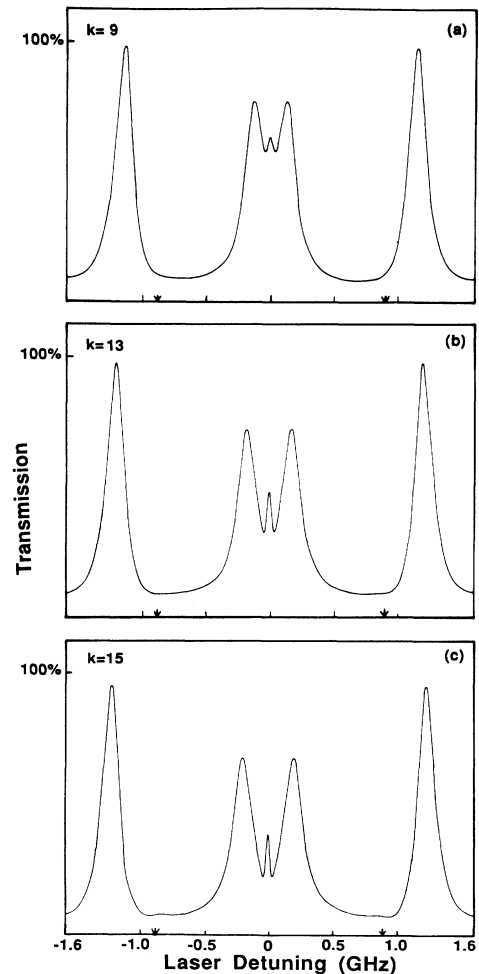The k values were varied to obtain close matching of

FIG. 7. Simulated transmission of a Fabry-Perot étalon vs laser detuning as a function of atomic density term k (a) $k = 9$, (b) $k = 13$, and (c) $k = 15$. As in Fig. 6, the laser detuning is from the midtransitions frequency and the position of each transition is marked by an arrow. The peak intracavity Rabi frequency is 180 MHz. The atomic parameters are the same as Fig. 6 and the cavity characteristics are finesse$=5$ and free-spectral range$=980$ MHz.

the absorption features of the sequences. From Eq. (52), the atomic density range is estimated at 1.3×10^{11} cm^{-3} to 2.1×10^{11} cm^{-3} which gives a temperature range for the simulated sequence of approximately 147–154 °C. Again, this is in acceptable agreement with the temperature range for the experimental sequence.

In the simulated data, the outer-cavity transmission peaks have about a 15% greater frequency separation from the triple-peaked profile than is observed in the experimental transmissions. Variation of the cavity finesse and free-spectral range effects this separation but then also changes the relative widths of the profiles. However, since the transformations (48) are valid only for the laser frequency tuned in between the two transition frequencies,[12]

the discrepancy in the position of the outer peaks is not surprising.

It is interesting to note that there is a slight distortion of the base of the inner side of the simulated outer-cavity profiles which also appears in the majority of the experimentally recorded peaks. These regions are close to the frequencies of the two atomic transitions from the ground states.

The behavior of the Fabry-Perot étalon transmission can be explained in terms of the macroscopic susceptibility whose real and imaginary parts are plotted in Fig. 8. For a cavity tuned to f_M, it can be seen that when the laser is detuned such that $\delta < 0$, then, since the dispersion is positive [Fig. 8(a)], it is possible to meet the condition

$$\delta = -\tfrac{1}{2}\omega_M \chi' \tag{53}$$

from Eq. (51), provided the density (k) is large enough. Thus, from Eq. (41), θ can be zero again and another transmission peak exists close to the f_M. Similarly, there will be another peak symmetrically placed for $\delta > 0$. Furthermore, since the width of the observed transmission peak depends on the rate of change of the phase at $\theta = 0$, the central feature of the triple-peaked profile should be narrower than the other peaks of that profile as the slope of the dispersion curve is greatest at $\delta = 0$. Also, as this slope increases with increasing density, the central feature will become narrower.

A physical description of the phenomenon can be given. Atoms of the velocity classes which have Doppler shifts so that they are near resonant with the radiation traveling

in one direction only are strongly pumped to the nonresonant ground state and so do not contribute significantly to the macroscopic susceptibility of the medium. However, those atoms which have Doppler shifts close to half the ground-state splitting interact resonantly with both forward and backward traveling light. Their sharp resonance behavior leads to enhanced absorption and rapidly changing dispersion about the "resonance" frequency f_M. The cavity resonance condition depends on the intracavity optical path length, and hence on the dispersion of the medium. Conditions here are such that as the laser is detuned from f_M, the laser–empty-cavity detuning frequency is offset by the change in the optical path length due to the rapidly changing dispersion. Effectively the cavity is frequency shifted back into resonance with the laser after a small-laser detuning. Since the phenomenon can happen for positive or negative detunings, the three-peaked profile is created.

The relative degree of transmission of the cavity peaks is reflected by the medium absorption as depicted in Fig. 8(b). As stated, the greatest contribution to the nonlinear absorption centered on f_M comes from those atoms with a Doppler shift of exactly, or very close to, half the ground-states frequency splitting. We have subsequently performed experiments using the same Fabry-Perot étalon but with an intracavity medium of an array of sodium atomic beams.[25] The collimation of the beams was such that the residual Doppler width was reduced well below the ground-state splitting and both ground-state hyperfine transitions were clearly resolved. Under these conditions, there is no longer a velocity group of atoms which can have both transitions simultaneously in resonance with the intracavity field. As was expected, the triple-peaked phenomenon was not observed.

V. SUMMARY

The unusual behavior of the transmission of low-finesse optical cavities filled with sodium vapor as a function of the injected-field frequency which is swept through a D transition has been studied under conditions below threshold for optical bistability. The experimental data could not be explained in terms of a two-state model for the energy levels associated with the atomic transitions and so a theoretical description for each cavity configuration was developed using the Λ-type, three-state model. While the salient features of the transmission data for the ring cavity are reproduced using this theoretical model, there is disagreement in the degree of absorption of the cavity peak tuned to the frequency midway between the atomic transitions. However, in all aspects, the theoretical calculations for the Fabry-Perot étalon case incorporating the three-state model demonstrate good agreement with the corresponding experimental data.
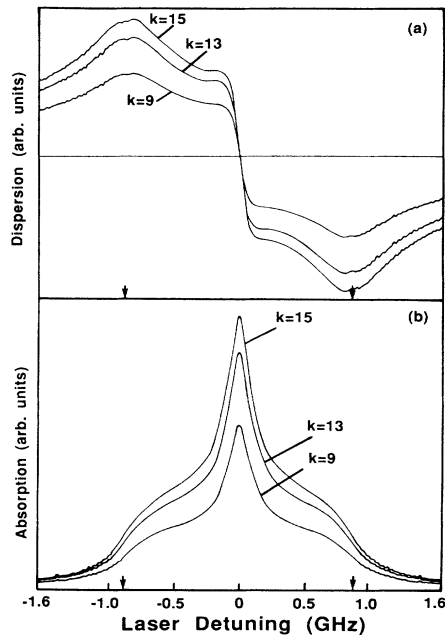

FIG. 8. The macroscopic susceptibility of the Fabry-Perot étalon intracavity medium as functions of laser detuning. (a) Dispersion, and (b) absorption. The relevant k parameter values are as in Fig. 7 and the Rabi frequency is 180 MHz.

ACKNOWLEDGMENTS

One of us (W.E.S.) wishes to acknowledge Griffith University for financial support.

APPENDIX

The derivation of the transmission of the Fabry-Perot étalon, Eq. (39), follows the standard treatment of adding all of the individual transmitted fields.[26] However, with an absorbing medium, the field is reduced by $\exp(-KL)$ for each pass through the medium between the mirrors, which are separated by distance L. Hence, we can write the transmitted field as

$$E_T = E_I t^2 e^{-KL} + E_I t^2 r^2 e^{-3KL} e^{i\beta}$$
$$+ E_I t^2 r^4 e^{-5KL} e^{i2\beta} + \cdots , \tag{A1}$$

where E_I is the amplitude of the incident field, t is the fraction of the field transmitted through each mirror, r is the fraction of the field reflected at each mirror, and β is the round-trip phase shift of the field. For simplicity, r and t are taken to be the same for each mirror. From Eq. (A1), E_T is

$$E_T = \frac{E_I(1 - r^2)e^{-KL}}{1 - r^2 e^{-2KL} e^{i\beta}} , \tag{A2}$$

where the relation

$$t^2 = 1 - r^2 \tag{A3}$$

has been used. The transmitted intensity is found from Eq. (A2) by

$$I_T = E_T E_T^* , \tag{A4}$$

where the asterisk represents the complex conjugate. The transmission of the cavity is the ratio of the transmitted intensity to the incident intensity,

$$I_r = I_T / E_I^2 , \tag{A5}$$

giving

$$I_r = \frac{e^{-2KL}(1 - r^2)^2}{(1 - r^2 e^{-2KL})^2 + 4r^2 e^{-2KL} \sin^2(\beta/2)} . \tag{A6}$$

By defining the fraction of intensity reflected at each mirror as R, and the half-round-trip phase shift as θ, Eq. (A6) is written as

$$I_r = \frac{A(1 - R)^2}{(1 - RA)^2 + 4RA \sin^2\theta} , \tag{A7}$$

where A is the attenuation coefficient

$$A = \exp(-2KL) . \tag{A8}$$

Equation (A7) is Eq. (39) of the text. The phase shift and the absorption are related to the real η and imaginary κ parts of the refractive index, respectively, by

$$\theta = \omega_L \eta L / c , \tag{A9}$$

$$K = \omega_L \kappa / c . \tag{A10}$$

The refractive index is related to the susceptibility by the relationships[27]

$$\eta^2 - \kappa^2 = 1 + \chi' , \tag{A11}$$

$$2\eta\kappa = \chi'' . \tag{A12}$$

To a good approximation, under the conditions of this experiment, $\chi'' \ll \chi' \ll 1$. Then,

$$\eta \simeq 1 + \tfrac{1}{2}\chi' , \tag{A13}$$

$$\kappa \simeq \chi''/2 . \tag{A14}$$

As well, the free-spectral range Φ of the cavity is related to the distance L between the mirrors by

$$\Phi = c/2L . \tag{A15}$$

Substituting Eqs. (A13) and (A15) into Eq. (A9) yields

$$\theta \simeq \omega_L(1 + \tfrac{1}{2}\chi')/(2\Phi) . \tag{A16}$$

If the cavity is considered tuned to ω_M, then, neglecting multiples of 2π, the phase shift can be written as

$$\theta = (\omega_L - \omega_M + \tfrac{1}{2}\omega_L \chi')/(2\Phi) . \tag{A17}$$

Substituting Eqs. (A14), (A15), and (A10) into Eq. (A8) gives

$$A = \exp[-\omega_L \chi''/(2\Phi)] . \tag{A18}$$

Finally, assuming that the laser is never greatly detuned from ω_M, Eqs. (40) and (41) are obtained, that is,

$$A = \exp[-\omega_M \chi''/(2\Phi)] , \tag{A19}$$

$$\theta = (\delta + \tfrac{1}{2}\omega_M \chi')/2\Phi . \tag{A20}$$

---

*Present address: Max-Planck-Institut für Quantenoptik, D-8046 Garching, Federal Republic of Germany.

[1] H. M. Gibbs, S. L. McCall, and T. N. C. Venkatesan, Phys. Rev. Lett. 36, 1135 (1976).

[2] W. J. Sandle and A. Gallagher, Phys. Rev. A 24, 2017 (1981).

[3] F. T. Arecchi, G. Giusfredi, E. Petriella, and P. Salieri, Appl. Phys. B 29, 79 (1982).

[4] J. Mlynek, F. Mitschke, R. Deserno, and W. Lange, Appl. Phys. B 28, 135 (1982).

[5] J. Mlynek, F. Mitschke, R. Deserno, and W. Lange, Phys. Rev. A 29, 1297 (1984).

[6] W. E. Schulz, W. R. MacGillivray, and M. C. Standage, Opt. Commun. 45, 67 (1983).

[7] F. Mitschke, R. Deserno, J. Mlynek, and W. Lange, Opt. Commun. 46, 135 (1983).

[8] S. Cecchi, G. Giusfredi, E. Petriella, and P. Salieri, Phys. Rev. Lett. 49, 1928 (1982).

[9] W. J. Sandle and M. W. Hamilton, in Proceedings of the Third New Zealand Symposium on Laser Physics, edited by J. D. Harvey and D. F. Walls (Springer, Berlin, 1983), p. 54.

[10] F. Mitschke, J. Mlynek, and W. Lange, Phys. Rev. Lett. 50, 1660 (1983).

[11] W. R. MacGillivray, in Proceedings of the Third New Zealand Symposium on Laser Physics, edited by J. D. Harvey and D. F.

Walls (Springer, Berlin, 1983), p. 41.

[12]D. T. Pegg and W. E. Schulz, Opt. Commun. **53**, 274 (1985).

[13]J. A. Abate, Opt. Commun. **10**, 269 (1974).

[14]G. Orriols, Nuovo Cimento B **53**, 1 (1979).

[15]I. V. Hertel and W. Stoll, in *Advances in Atomic and Molecular Physics,* edited by D. R. Bates and B. Bederson (Academic, New York, 1977), p. 137.

[16]W. E. Schulz, W. R. MacGillivray, and M. C. Standage, Phil. Trans. Soc. London, Ser. A **313**, 417 (1984).

[17]R. M. Whitley and C. R. Stroud, Phys. Rev. A **14**, 1498 (1976).

[18]D. F. Walls and P. Zoller, Opt. Commun. **34**, 260 (1980).

[19]L. Allen and J. H. Eberly, *Optical Resonance and Two-Level Atoms* (Wiley, New York, 1975), p. 79.

[20]L. A. Lugiato, Contemp. Phys. **24**, 333 (1983).

[21]R. Bonifacio and L. A. Lugiato, Lett. Nuovo Cimento **21**, 505 (1978).

[22]R. Bonifacio and L. A. Lugiato, Opt. Commun. **19**, 172 (1976).

[23]A. T. Rosenberger, L. A. Orozco, and H. J. Kimble, Phys. Rev. A **28**, 2569 (1983).

[24]H. J. Carmichael and G. P. Agrawal, Opt. Commun. **34**, 293 (1980); see also E. Abraham and S. D. Smith, Rep. Prog. Phys. **45**, 815 (1982), and references therein.

[25]W. E. Schulz, Ph. D thesis, Griffith University, 1985.

[26]M. Born and E. Wolf, *Principles of Optics,* 5th ed. (Pergamon, New York, 1975), p. 323.

[27]R. Loudon, *The Quantum Theory of Light,* 2nd ed. (Clarendon, Oxford, 1983), p. 25.